Heterogeneous flexibility can contribute to chromatin segregation in the cell nucleus

Martin Girard,[1] Monica Olvera de la Cruz,[2] John F. Marko,[3] and Aykut Erbaş[4]
[1]*Max-Planck Institute for Polymer Research, 55128 Mainz, Germany*
[2]*Department of Materials Science and Engineering, Department of Chemistry, Department of Chemical and Biological Engineering, and Department of Physics and Astronomy, Northwestern University, Evanston, Illinois 60208, USA*
[3]*Department of Molecular Biosciences and Department of Physics and Astronomy, Northwestern University, Evanston, Illinois 60208, USA*
[4]*UNAM-National Nanotechnology Research Center and Institute of Materials Science & Nanotechnology, Bilkent University, Ankara 06800, Turkey*

(Received 18 October 2023; accepted 29 May 2024; published 3 July 2024)

The highly and slightly condensed forms of chromatin, heterochromatin and euchromatin, respectively, segregate in the cell nucleus. Heterochromatin is more abundant in the nucleus periphery. Here we study the mechanism of heterochromatin segregation by modeling interphase chromosomes as diblock ring copolymers confined in a rigid spherical shell using molecular dynamics simulations. In our model, heterochromatin and euchromatin are distinguished by their bending stiffnesses only, while an interaction potential between the spherical shell and chromatin is used to model lamin-associated proteins. Our simulations indicate that in the absence of attractive interactions between the nuclear shell and the chromatin, most heterochromatin segregates towards the nuclear interior due to the depletion of less flexible heterochromatin segments from the nuclear periphery. This inverted chromatin distribution,which is opposite to the conventional case with heterochromatin dominating at the periphery, is in accord with experimental observations in rod cells. This "inversion" is also found to be independent of the heterochromatin concentration and chromosome number. The chromatin distribution at the periphery found *in vivo* can be recovered by further increasing the bending stiffness of heterochromatin segments or by turning on attractive interactions between the nuclear shell and heterochromatin. Our results indicate that the bending stiffness of chromatin could be a contributor to chromosome organization along with differential effects of HP1α-driven phase segregation and of loop extruders and interactions with the nuclear envelope and topological constraints.

DOI: 10.1103/PhysRevE.110.014403

I. INTRODUCTION

In the several-micron-diameter nuclei of eukaryotic cells, centimeter-long DNA molecules are three-dimensionally organized via a dense array of structural nucleic acid-binding proteins. Among those proteins, histone proteins organize DNA chains into chromatin fibers by forming quasi-one-dimensional arrays of nucleosomes [1]. Recent computational and experimental studies show that variations in nucleosome arrangement along the chromatin can induce inhomogeneities in chromatin morphology [2–5], making chromatin a highly heterogeneous polymer that can be modeled as a copolymer chain [6,7].

A linear copolymer can be composed of more than one distinct chemical or structural unit. These units can bear attractive or repulsive interactions towards each other or solvent, leading to their local segregation under appropriate physio-chemical conditions [8]. For example, block copolymers can undergo nanoscopic phase segregation [9] while random copolymers lead to local segregation of domains of different compositions [10]. In a typical eukaryotic cell, the nuclear chromatin copolymer is thought to be mesoscale segregated [6,11]. Chromatin sections with densely packed nucleosomes, termed heterochromatins and associated with gene silencing, tend to be found near the nuclear periphery, whereas more transcriptionally active chromatin with loosely packed nucleosomes (i.e., euchromatin) occupies the more central region of the nucleus [12–15]. Domains of constitutive heterochromatin are known to be dependent on the nucleosome-binding protein HP1. These domains are thought to possibly be controlled by dimerization of HP1 molecules bound to their targets and possibly by a tendency for HP1 to phase separate, which has been observed *in vitro* [16–18]. However, the precise mechanism underlying heterochromatin domain formation *in vivo* remains controversial [19–21]. The localization of heterochromatin at the nuclear periphery is also attributed to attractive interactions between the confining shell and chromatin provided by proteins, including lamin B receptors (LBRs) and lamin A/C [22–24]. In accord with this picture, the absence of such proteins that tend to localize heterochromatin to the nuclear periphery results in the coalescence of heterochromatin in the nuclear interior [6,25–29].

Aside from chemical heterogeneity, another key physical property of copolymers that can influence the segregation is the effective persistence length, l_p. The persistence length characterizes the response of a polymer segment to bending fluctuations and is defined as the smallest length scale below which the polymer behaves like a stiff rod. While a homogeneous polymer chain (e.g., a naked DNA composed of $\gg 100$ base pairs) has a uniform persistence length of $l_p \approx 50$ nm along its contour length, a copolymer, such as chromatin, can exhibit a nonuniform persistence length profile

along its contour length. Chromatin is heterogeneous, with a high degree of biochemical and structural complexity [30,31], which could contribute to the variation of effective stiffness along the fiber. Most simply, this can occur via variation in the cross-sectional area of the chromatin fiber, which, even without additional physiochemical effects, would be expected to lead to variation in bending stiffness (e.g., via $l_p \approx a^4$ where a is the cross-sectional radius).

Values measured for the persistence length of chromatin fiber lie in a broad range of values from $l_p \approx 30$ nm to $l_p \approx 300$ nm [32–34]. One possibility for this variation could be technical difficulties in handling chromatin or in performing persistence length measurements on such a complex supramacromolecular complex. Nevertheless, this wide range of values may also indicate true heterogeneity, leading to the hypothesis that heterogeneous chromatin flexibility may provide a mechanism for nuclear chromatin organization, in concert with other energetic demixing interactions.

It is known that inhomogeneous flexibility along a polymer can affect its phase behavior independent of affinity effects [35–37]. Furthermore, the hypothesis that the mechanical flexibility of chromatin can contribute to nuclear organization via entropic effects has been previously considered. Monte Carlo (MC) simulations of relatively short (i.e., $N = 50$ effective monomers) homo-polymer rings of model heterochromatin and euchromatin in spherical confinement showed a concentration-dependent segregation mechanism [38]. Heterochromatin rings were shown to weakly segregate towards the nuclear periphery for volume fractions around 10% to minimize segmental bending energy [38]. However, it is not clear whether such an effect will occur if the hetero- and euchromatin sections are joined together in the form of a copolymer. Furthermore, the volume fraction of interphase chromatin is usually higher than 10% and also varies for different cell types [34]; the interplay between the volume fraction and stiffness variation and their possible effects on nuclear organization remains to be studied.

In order to study how mechanical heterogeneity along chromatin polymer can affect nuclear organization, we model interphase chromosomes as diblock ring copolymers by using a generic coarse-grained polymer model [39–42] confined in a rigid spherical shell. The long chromatin chains (i.e., $N = 1000$) are composed of prescribed lengths of heterochromatin and euchromatin blocks, in which the only difference between heterochromatin and euchromatin blocks is in their flexibility such that heterochromatin is always less flexible than euchromatin [Fig. 1(a)]. We use this setup to model the conventional (i.e., heterochromatin is at the periphery and euchromatin is in the nuclear interior) and inverted nuclear chromatin organization to assess if flexibility difference and interaction with the confining shell alone (i.e., nuclear envelope, NE) would be enough to obtain those organization patterns. Our molecular dynamics (MD) simulations show that when there is no attraction between the inner surface of the shell and chromatin, the majority of heterochromatin localizes in the nuclear interior by depleting euchromatin, in accord with the experimental observations of heterochromatin inversion [27,28]. However, we also find that weak attractive interactions (i.e., on the order of thermal energy k_BT) between heterochromatin and shell can reverse the heterochromatin inversion by depleting heterochromatin from the nuclear interior. The conventional nuclear organization (more heterochromatin at the nuclear periphery) is also obtained if the persistence length of heterochromatin is on the order of the dimension of the shell.

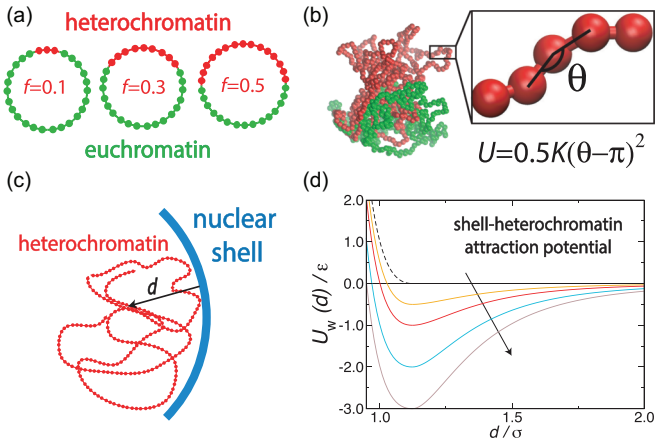

FIG. 1. Simulation model. (a) The schematics of individual chromatin rings with various fractions of heterochromatin content, f. (b) An arbitrary simulation snapshot showing an isolated single chromatin chain with $f = 0.5$, and the schematics of the bending potential applied to heterochromatin (red beads) only to alter its persistence length [Eqs. (4) and (5)]. (c) The schematics of the attractive potential between heterochromatin beads and the rigid confining shell. (d) The plot of the attractive potential, Eq. (1), as a function of the rescaled distance from the shell, d/σ. The arrow indicates the direction of increasing attraction strength for various values of χ. The dashed curve refers to the WCA potential.

II. METHODS

In our MD simulations, interphase chromosomes are modeled as bead-spring chains, a model widely used to study large-scale and long-time behavior of biological and synthetic polymers [42] [Figs. 1(a) and 1(b)]. We confined a number (n_{ch}, ranging from 6 to 16) unconcatenated copolymers with ring topology to the interior of a rigid sphere as a model of nuclear confinement. The ring topology has been shown to model chromosome territories successfully [39,40,43] and eliminates the role of the position of the heterochromatin block within the polymer (as would be the case for a linear polymer). Each chain is composed of $N = 1000$ beads of size σ. Our chromatin model is highly coarse-grained: each bead represents roughly 10 nucleosomes, resulting in around $\approx 1.6 \times 10^6$ base pairs (bps) per chain (160 bp per nucleosome) per chromosome, with therefore a total genome size of up to 3×10^7 bps. The radius of the confining shell is $R = 20\sigma$, which leads to various volume fractions $\phi = n_{ch}N\sigma^3/(8R^3)$ ranging between $10\% \lesssim \phi \lesssim 25\%$. Thus, our systems may correspond to weak (e.g., yeast) and moderate (e.g., *Drosophila*) confinement levels [41]. Nonbonded interactions between beads are described by an Ashbaugh-Hatch potential [44],

$$U_{ij} = \begin{cases} \Phi_{LJ}(r) + \varepsilon(1 - \chi_{ij}) & r < 2^{1/6}\sigma \\ \chi_{ij}\Phi_{LJ}(r) & 2^{1/6}\sigma < r < 2.5\sigma \end{cases}, \quad (1)$$

where $\Phi_{\rm LJ}(r)$ is the usual 12-6 Lennard-Jones (LJ) potential,

$$\Phi_{LJ} = 4\varepsilon[(\sigma/r)^{12} - (\sigma/r)^{6}] \tag{2}$$

where the energy scale is $\varepsilon = k_{\rm B}T$. Ideal mixture conditions in an athermal solvent limit are obtained by setting $\chi = 0$.

Interactions between the inner surface of the sphere and all beads were also modeled by the above-mentioned Ashbaugh-Hatch potential [Fig. 1(c)] to avoid the diffusion of monomers outside of the sphere. To model the attractive interactions between the heterochromatin and NE, the value of the attraction strength is varied between $0.1 \leqslant \chi \leqslant 3.0$ [Fig. 1(d)].

Springs connecting two adjacent chain beads separated by a distance r are taken care of by the finitely extensible nonlinear elastic (FENE) potential, which does not allow bond crossing,

$$U_F = -0.5K_F r_0^2 \ln[1 - (r/r_0)^2], \tag{3}$$

where the bond strength is $K_F = 30\varepsilon/\sigma^2$, and the maximum bond stretch is $r_0 = 1.5\sigma$. Equation (3) provides a statistical bond length of $b \approx 1\sigma$.

To construct the heterogeneity of flexibility for our heteropolymers, a harmonic angular potential, which energetically penalizes the bending of heterochromatin segments, is used to control the flexibility of a prescribed fraction, f, of each chain [Figs. 1(a) and 1(b)]. By varying f as $0.1 \leqslant f \leqslant 0.5$, various heterochromatin contents are obtained. The form of the angular potential is

$$U = 0.5K(\theta - \pi)^2, \tag{4}$$

where the heterochromatin spring constant is $K = 2\varepsilon/\text{rad}^2$ unless noted otherwise, and the angle between three consecutive beads of the corresponding chain segment is θ [Fig. 1(b)] (below, we will suppress the dimensionless factor of rad^2 in the value of K). The potential, Eq. (4), is applied only to heterochromatin blocks. For heterochromatin, K may be related to $l_{\rm p}$ as [45]

$$l_{\rm p}^{\rm htc} \approx Kb/\varepsilon. \tag{5}$$

We test the above expression by using linear chains of $N = 100$ monomers and obtain persistence lengths $l_{\rm p}^{\rm htc} \approx 1.43\sigma$ with $K/\varepsilon = 2$ and $l_{\rm p}^{\rm euc} \approx 0.93\sigma$ with $K = 0$ for heterochromatin and euchromatin, respectively (see Supplemental Material [46], Fig. S1), leading to a ratio $l_{\rm p}^{\rm htc}/l_{\rm p}^{\rm euc} = 1.5$

MD simulations were carried out using the HOOMD-blue molecular dynamics engine [47,48] with initial configurations built by the Hoobas molecular builder [49]. The simulation boxes were maintained at constant temperature by using a Langevin thermostat with a damping coefficient of $\gamma = \delta t$, where $\delta t = \sqrt{m\sigma^2/\varepsilon}$ is the LJ time unit with unit mass $m = 1$. The pressure exerted on the spherical confinement is too small to be accurately measured (see Supplemental Material [46], Fig. S2). A simulation time step of $\Delta t = 0.002\delta t$ was used. Polymer chains were prepared as circles followed by relaxation of a minimum of 10^7 MD steps. The 10^9 MD steps (i.e., $2 \times 10^6 \delta t$) were run for data production. The initial configuration of our polymer rings is not a well-mixed system. For entangled melts, the memory of this configuration may persist in our results [40,41]. However, simulating unentangled melts of ring polymers shows consistent effects as described here (see Supplemental Material [46]). Extending the simulation time to 2×10^9 steps does not qualitatively affect results (see Supplemental Material [46], Fig. S3).

Data were acquired every 10^4 MD steps. Visualization was done using OVITO [50] and VMD [51], while trajectory analyses were done using custom C++ codes. The VMD sphere scale in the snapshots was set to 0.6. Error bars were calculated via the standard deviation of the mean estimate and are not shown if they are smaller than the symbol size.

III. RESULTS

A. Heterochromatin concentration is higher at nuclear center in the absence of chromatin-shell attraction

Experiments on various cell types have established that in the absence of certain lamin-associated proteins, interphase heterochromatin mostly localizes in the nuclear interior [27,28]. This is in opposition to the general trend, in which the majority of heterochromatin resides near the NE [13,24]. The emergence of this so-called inverted distribution inside the nucleus requires a driving force that can sustain an asymmetric, rather than uniform, heterochromatin distribution. To investigate whether the mechanical heterogeneity along the chromatin polymer can by itself provide such segregation, we first consider in our simulations the scenario, in which there is no net attraction between the inner surface of the confining spherical shell and the chromatin. In this way, we mimic the experimental conditions where heterochromatin-shell interactions are weak [28]. Since in our simulations, heterochromatin and euchromatin monomers interact with the same pairwise potential, Eq. (1); i.e., all monomers are chemically identical, the equilibrium chromatin organization will be determined by the difference in the bending fluctuations of the two chromatin types.

First, we consider the case in which nuclear concentrations of heterochromatin and euchromatin are equal [i.e. each chromatin chain is composed of an equal number of heterochromatin and euchromatin monomers, $f = 0.5$; see Fig. 1(a)]. In this situation, there is no concentration bias towards either chromatin type. We take heterochromatin to be stiffer than euchromatin (i.e., $K/\varepsilon = 2$ in Eq. 4) [38]. This corresponds to heterochromatin having approximately 50% longer persistence length than the statistical segment length of euchromatin (i.e., $l_{\rm p}^{\rm htc}/l_{\rm p}^{\rm euc} \approx 1.5$; see Supplemental Material [46], Fig. S1).

To quantify the chromatin distribution across the nucleus, we calculate the radial concentration profiles for both heterochromatin and euchromatin monomers as a function of the rescaled distance from the nuclear center, r/R, by using our simulation trajectories (Fig. 2). The concentration profiles rescaled by total average concentration, ρ/ρ_0, exhibit a nonuniform behavior across the nuclear volume. Near the nuclear center (i.e., $r/R \to 0$), an increase of heterochromatin concentration is accompanied by a depletion of euchromatin regardless of volume fraction [Figs. 2(a) and 2(b)], similar to the experimentally observed inverted heterochromatin distribution [27,28]. At the nuclear center, the heterochromatin concentration is almost 50% higher than euchromatin [Figs. 2(a) and 2(b)], and this difference diminishes as $r/R \to$

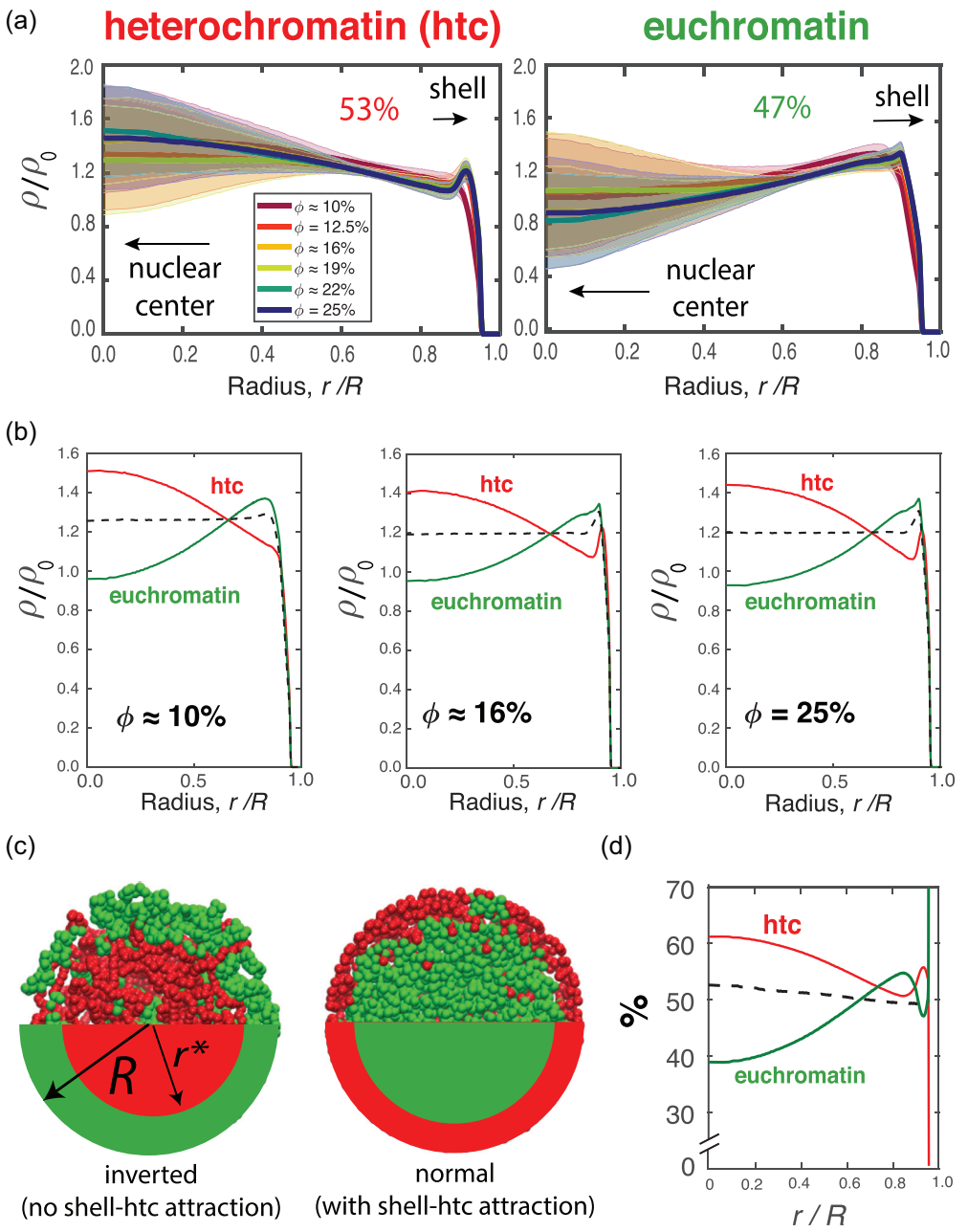

FIG. 2. Radial concentration profiles. (a) The normalized radial density profiles of heterochromatin and euchromatin as a function of the rescaled radial distance from the sphere center for various volume fractions ϕ for heterochromatin stiffness of $K/\varepsilon = 2$. The heterochromatin fraction is $f = 0.5$. The numbers indicate percentages of respective chromatin types in the central region (see text for details). (b) The normalized radial density profiles are shown in A for three volume fractions. Error bars, as in (b), are not shown for clarity. Dashed curves are the control simulations with $K/\varepsilon = 0$ (i.e., all euchromatin). (c) Representative simulation snapshots showing the cross section of the chromatin-filled shells, in which $n_{ch} = 6$ chains are spherically confined for vanishing and nonvanishing surface-heterochromatin attraction strengths. Heterochromatin and euchromatin are represented by red and green beads/shades, respectively. (d) Relative occupancy of two chromatin types across the nucleus.

1. Note that the density fluctuations (color bands indicate the standard deviation of the mean estimate) in Fig. 2(a) increase as $r/R \to 0$ due to the smaller number of monomers near the center. Nevertheless, as compared to the all-euchromatin scenario [i.e., $K = 0$, dashed curves in Fig. 2(b)], our quantitative observations of central heterochromatin coalescence is robust within the simulation time window, which is approximately three times the theoretical relaxation time of a linear chain with equal length [52].

This inverted heterochromatin distribution, with heterochromatin at the nuclear interior, is consistent with the enhanced euchromatin concentration near the nuclear periphery [Figs. 2(a) and 2(b)]. While heterochromatin concentration is lower than euchromatin at the nuclear boundary,

heterochromatin localization exhibits a concentration-dependent behavior [Fig. 2(b)]. A previous study has reported such concentration-dependent heterochromatin enhancement near the nuclear periphery [38]. Accordingly, above the volume fractions of $\phi \approx 10\%$, less flexible heterochromatin homopolymer chains localize near the large curvature regions at the periphery to minimize the energy penalty against bending [38]. In Figs. 2(a) and 2(b), we also observe this trend with our heteropolymer chromatin chains as the volume fraction is increased from $\phi \approx 10\%$ to $\phi \approx 25\%$ at $r/R \to 1$. However, in our case, the peripheral heterochromatin localization at the shell does not strongly affect the concentration difference in the nuclear interior between heterochromatin and euchromatin [Figs. 2(a) and 2(b)]. Importantly, unconcentrated ring polymers reported in Ref. [38] result in relatively low chromatin density at the nuclear interior, unlike copolymers considered here, due to the unconnected nature of heterochromatin and euchromatin chains.

The central heterochromatin coalescence that we quantify via concentration profiles is also evident from the representative snapshots taken from the final frames of corresponding MD simulations [Fig. 2(c)]. The snapshot on the left-hand side of Fig. 2(c) demonstrates the chromatin organization without shell-heterochromatin attraction. A visual inspection reveals the systematic localization of the heterochromatin (green) towards the nuclear center and increased euchromatin (red) occupation at the nuclear periphery. This inverted chromatin organization can be compared to the snapshot from a separate simulation, for which the attraction between the shell and heterochromatin is introduced [the snapshot on the right-hand side of Fig. 2(c)]. As we will discuss further in the next sections, the shell-chromatin attraction increases the concentration of the heterochromatin at the periphery while enhancing euchromatin presence in the nuclear interior, which is the conventional nuclear organization [53,54].

To obtain further insight into the higher concentration of heterochromatin near the nuclear center as compared to euchromatin, we calculate the relative occupancy of the two chromatin types, $n_h(r)/[n_h(r)+n_e(r)]$ and $n_e(r)/[n_h(r)+n_e(r)]$, where $n_h(r)$, and $n_e(r)$ are the number of heterochromatin and euchromatin beads, respectively, at a radial position $0 < r < R$. The sum of the two relative concentrations is unity. The relative concentration profile for $\phi \approx 10\%$ in Fig. 2(d) confirms the trend of central heterochromatin coalescence, and the depletion of euchromatin from the interior: On average, near the center of the nucleus, the probability of a heterochromatin bead encountering another heterochromatin bead is significantly higher than a euchromatin bead, and this trend is in stark contrast with the control [i.e., $K/\varepsilon = 0$, the dashed curve in Fig. 2(d)], for which there is no flexibility difference along the chromatin.

Overall, our MD simulations can reproduce qualitatively the experimentally observed central heterochromatin coalescence [27,28] in the case where the only difference between heterochromatin and euchromatin is heterochromatin being stiffer by about a factor of two (i.e., $l_p^{htc}/l_p^{htc} \approx 1.5$), in the otherwise symmetric situation where there are equal amounts of heterochromatin and euchromatin ($f = 0.5$).

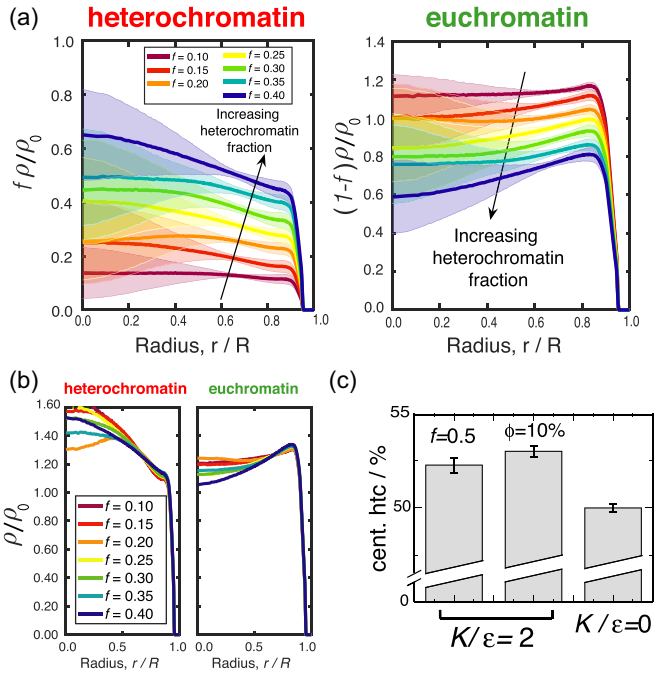

FIG. 3. (a) Radial concentration profiles for various heterochromatin and euchromatin contents f at a volume fraction of $\phi \approx 10\%$. The difference in flexibility is $K/\varepsilon = 2$ for all cases. The data are normalized by the rescaled concentrations to indicate the absolute difference. Arrows indicate the direction of increasing f. (b) Concentration profiles normalized by the average concentration of respective chromatin types. Error bars are not shown for clarity. (c) The percentage of heterochromatin within the central region of the nucleus averaged over various values of ϕ and f cases as compared to all-euchromatin case (i.e., $K/\varepsilon = 0$). The bar on the left is averaged over all volume fraction cases (i.e., $\phi = 10, 16, 25\%$ cases at a fixed $f = 0.5$, and the bar at the center is averaged over all f cases for a fixed $\phi = 10\%$.

B. Central heterochromatin localization is robust with varied relative heterochromatin content

The results for the prior section considered the hetero/euchromatin symmetric situation $f = 0.5$, where in the absence of chromatin-shell interactions, the heterochromatin concentration is higher than euchromatin in the nuclear interior (Fig. 2). The next question is how this result is affected by the asymmetry $f \neq 0.5$, which is generally the case that will be encountered *in vivo*, with this asymmetry varying between cell types or even from cell to cell within a single cell type. For instance, for fully differentiated mammalian cells, roughly 40% of chromatin carry heterochromatin marks [22], and this fraction tends to be lower for embryonic stem cells [55]. Aging cells can exhibit a time-dependent loss of heterochromatin [56]. Given these data, we next focus on the case of heterochromatin fraction $f < 0.5$ (Fig. 3) to study the robustness of the central coalescence phenomenon we observed for $f = 0.5$. As the value of f is decreased, so does the total heterochromatin concentration relative to that of euchromatin [Fig. 3(a)]. However, the overall trend of the concentration profiles is nearly identical to the $f = 0.5$ case (Fig. 2). The concentration

of heterochromatin remains higher near the center than the periphery, and euchromatin occupation continues to be suppressed in the nuclear interior [Fig. 3(a)]. Again, rescaling heterochromatin and euchromatin concentrations by their average concentrations ρ_0, the general trend is that regardless of heterochromatin content, in the absence of anchoring interactions with the nuclear shell, heterochromatin concentrates near the nuclear center relative to euchromatin [Fig. 3(b)].

To obtain a quantitative measure of segregation, we calculate the cumulative heterochromatin concentration in the nuclear interior by dividing the nuclear volume into peripheral and central regions [Fig. 2(c)]. To carry this out in an as unbiased manner as possible, we determined the central/peripheral boundary r^* as the radius for which the overall chromatin concentration is equally distributed into central and peripheral regions in the flexibility-symmetric case $K/\varepsilon = 0$ [Fig. 3(c), rightmost bar]. Once we break flexibility symmetry ($K/\varepsilon \neq 0$), the occupation symmetry is broken, leading to a total heterochromatin accumulation in the central and peripheral regions of $53 \pm 0.2\%$ and $47 \pm 0.2\%$, respectively, which confirms that the majority of the heterochromatin localizes in the nuclear interior [Fig. 3(c), $f = 0.5$, $\phi = 0.1$, leftmost bar]. While one might consider this heterochromatin accumulation in the nuclear interior to be weak (6% higher in the central region versus peripheral), this difference is robust, persisting across a range of values of f and ϕ, and exhibits a systematic deviation from the control simulations, in which there is no flexibility difference between heterochromatin and euchromatin [Fig. 3(c), rightmost bar].

We note that the definition of r^* in using the bending-symmetric case $K = 0$ is important: in particular, choosing the peripheral/central equal-volume division radius $r^*_{\mathrm{eq}} = R/2^{1/3} \approx 0.8$ leads to a chromatin amount bias even for the symmetric case $K/\varepsilon = 0$ (Supplemental Material [46], Fig. S4), likely due to the local osmotic depletion of monomers from the shell surface.

C. Large heterochromatin stiffness reduces and inverts central segregation via geometrical constraint of bending

Our simulations with heterochromatin bending rigidity $K/\varepsilon = 2$ lead to a segregation similar to that observed experimentally in systems lacking chromatin-NE attractions (Figs. 2 and 3). The difference in bending rigidity between heterochromatin and euchromatin can be considered to be weak since the bending length scale of both types of chromatin is small compared to the nuclear size ($l_{\mathrm{p}} \ll R$). We decided to find out what would happen as the heterochromatin stiffness is increased out of this regime. We vary the flexibility difference between $K/\varepsilon = 0.5$ and $K/\varepsilon = 15$ [Fig. 4(a)]. Since the K/ε parameter is proportional to the persistence length of the heterochromatin [Eq. (5)], this range probes heterochromatin persistence lengths up to the nuclear size. In addition to being theoretically important, such situations may not be entirely experimentally irrelevant since intermediate values of K/ε can be realized experimentally using DNA intercalators such as propidium iodide [57,58] or possibly by varied expressions of heterochromatic "reader" proteins such as HP1 [59] which may alter chromatin mechanics.

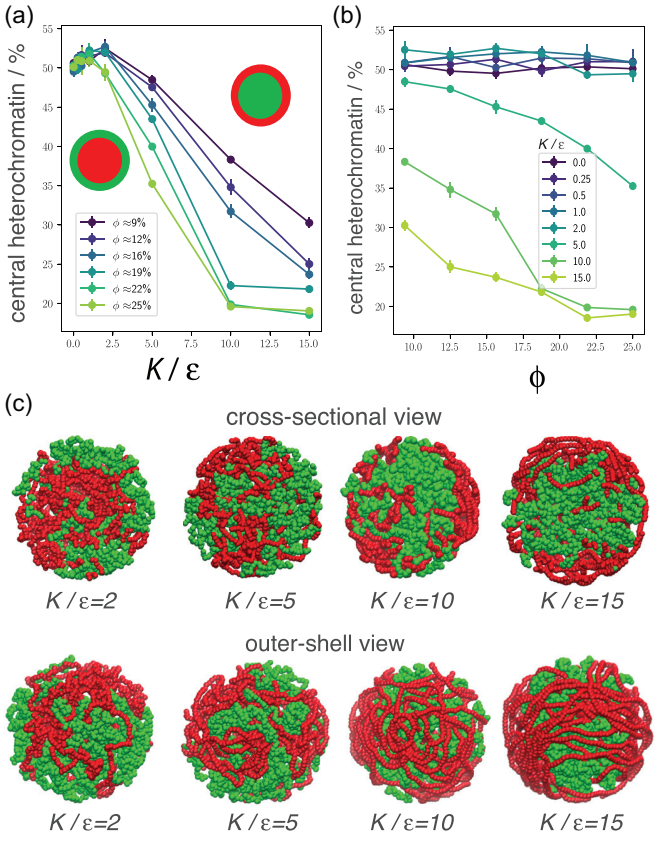

FIG. 4. Peripheral segregation of stiffer heterochromatin. (a) Heterochromatin accumulated in the central region for various volume fractions as a function of the stiffness parameter. (b) The same data as a function of the volume fraction but for various stiffness cases. (c) Cross-sectional and outer views of spherical shells for various stiffness values. The higher the K/ε value is, the stiffer the heterochromain is. Red and green beads are heterochromatin and euchromatin beads, respectively.

Figure 4(a) shows the heterochromatin accumulation in the central region as a function of K for various volume fractions. For weak differences in flexibility (i.e., $K/\varepsilon \approx 1$), most heterochromatin occupies the central region as before. As $K/\varepsilon \to 0$, the central coalescence of heterochromatin disappears. Notably, for $K/\varepsilon < 2$, this coalescence exhibits only a weak dependence on the volume fraction [Fig. 4(b)].

As the strength of the bending potential and, therefore, heterochromatin stiffness is increased further (i.e., to $K/\varepsilon = 5$), the heterochromatin segments exhibit a more pronounced localization at the periphery [Figs. 5(a) and 5(b) and Supplemental Material [46], Fig. S5)] At $K/\varepsilon = 10$, we observe the formation of circular heterochromatin loops strongly localized to the inner surface of the shell [Fig. 5(c)]. The circular segments disappear for $K/\varepsilon = 15$, and instead parallel, nematic-like heterochromatin segments cover the entire inner surface of the shell [Fig. 4(c)]. This is in accord with similar polymer layers reported for linear semiflexible chains confined in spherical volumes in the context of confinement-induced nematic phases [60]. Analysis of the nematic ordering suggests that local ordering (i.e., peripheral versus central ordering) plays a role in chromatin localization (see

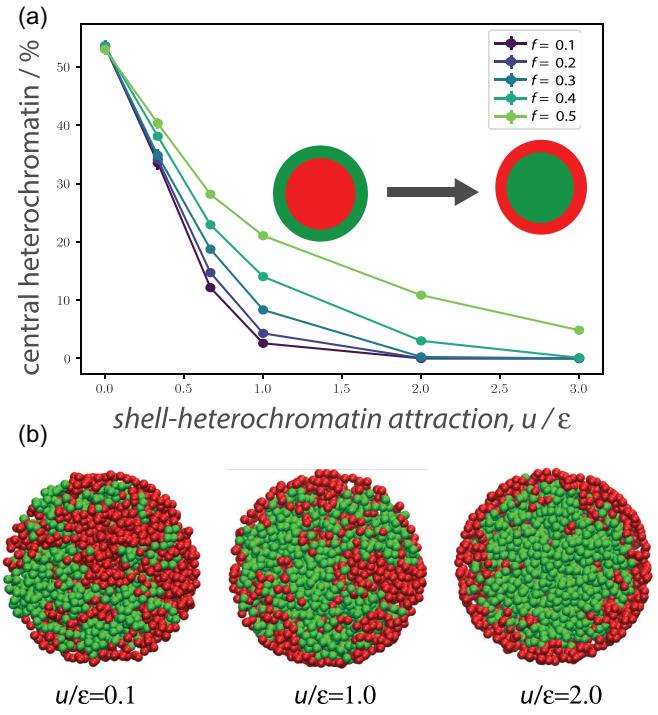

FIG. 5. Attraction between the shell and heterochromatin decreases heterochromatin segregation in the nuclear interior. (a) Percentage of heterochromatin within the central region for various heterochromatin fractions ranging from $f = 0.1$ to $f = 0.5$ as a function of the shell-heterochromatin interaction strength u/ε. (b) Cross-sectional views of the simulation snapshots from the respective equilibrium systems for $f = 0.5$ demonstrating heterochromatin segregation at $u/\varepsilon = 0.1$, 1.0, 2.0. In all cases $\phi \approx 10\%$ and $K/\varepsilon = 2$ (i.e., $l_p^{htc}/l_p^{euc} = 1.5$; see Supplemental Material [46], Fig. S1).

Supplemental Material [46], Fig. S6). Since local ordering is intrinsically tied to localization, this implies a nontrivial interplay of the two, which is beyond the scope of the present work. For biologically relevant (weak) differences in flexibility, our simulations indicate preferential heterochromatin localization in the nuclear interior. The observation of opposite effects in the limit of strong-bending rigidity indicates that our weak-bending results are in a regime where the nuclear radius is not controlling polymer distribution via direct constraint of semiflexible polymer bending.

D. Attraction between shell and heterochromatin reduces central localization

Having analyzed nuclear chromatin segregation within our minimal varied-stiffness model, we now add heterochromatin-NE attractive interactions. In reality, these interactions are mediated by lamin-associated proteins [15,28], which we approximate as a simple short-range potential in our simulations. While this is an extreme simplification of the complexity of chromatin-NE interactions, this model provides a measure of interaction strength needed to reverse the heterochromatin inversion.

In Fig. 5(a) we show heterochromatin accumulation within the central region as a function of the attraction strength u/ε for various heterochromatin contents f, for $\phi = 10\%$. As the attraction strength is increased, the heterochromatin concentration at the central region significantly decreases [Fig. 4(a)], and consequently, the peripheral-heterochromatin concentration increases, consistent with previous simulations and experiments [6,11,61,62]. At an attraction strength $u/\varepsilon \approx 0.5$, the peripheral and central heterochromatin concentration are approximately 50% [Fig. 3(a)]. The threshold attraction strength for this behavior is slightly weaker than the thermal energy scale k_BT, which highlights the entropic nature of the central coalescence that we observe here. Since the attraction strength is defined per bead, the total attraction acting on a segment composed of multiple beads is stronger than $1k_BT$. This indicates the possibility of polymer-based cooperativity, in which heterochromatin is adsorbed on the surface via a multivalent-binding mechanism [22].

As the attraction between the shell and heterochromatin is increased above the thermal energy, $u/\varepsilon > 1$, the fraction of surface-bound monomers increases regardless of overall heterochromatin content [Figs. 5(a) and 5(b)]. For the lowest amount of heterochromatin (i.e., $f = 0.1$), we observe a complete depletion of heterochromatin from the central region if the u/ε is increased 20-fold from $u/\varepsilon = 0.1$ to $u/\varepsilon = 2$. For higher values of f (e.g., $f = 0.5$), even for relatively high attraction strengths ($u/\varepsilon = 2$), we observe roughly 5% of the heterochromatin in the central region due to saturation of the surface by chromatin beads [Figs. 5(a) and 5(b)]. Notably, for $f = 0.5$, a *heterochromatin layer* is formed adjacent to the periphery due to overcrowding of the heterochromatin monomers there [rightmost snapshot of Fig. 4(b)].

Overall, our coarse-grained MD simulations show that when heterochromatin blocks of diblock chromatin polymers are less flexible, the majority of the heterochromatin localizes in the nuclear interior. This trend is nonmonotonic and can be reversed either by further increasing energy penalty for heterochromatin bending (Fig. 4) or, more relevant to heterochromatin *in vivo*, by inducing interactions between the confining shell and heterochromatin (Fig. 5).

IV. DISCUSSION

Our MD simulations show that a diblock ring copolymer, where two blocks are distinguished by their bending stiffness (i.e., persistence length), can exhibit segregation properties in spherical rigid confinement. Given that chromatin fiber can be highly heterogeneous due to variations in the 1D nucleosome packing, the segregation mechanism we demonstrate here could contribute to the 3D chromosome organization *in vivo* along with DNA-binding structural proteins and nonequilibrium processes. Below, we will discuss several scenarios where heterogeneous chromatin stiffness could have conceivable effects.

A. Heterogeneity in chromatin flexibility can contribute to nuclear organization

In our simulations, where chromatin is modeled as a diblock ring copolymer, demonstrate that only a small (e.g., a factor of less than 2) flexibility difference between the two chromatin types is enough to segregate stiffer heterochromatin towards the nuclear interior, away from the perimeter, if heterochromatin is not anchored to the NE (Figs. 2 and 3).

Importantly, this effect does not require any selective interaction between chromatin units, although such interactions are likely to strengthen this effect. This central heterochromatin localization effect is essentially independent of nuclear heterochromatin content (Fig. 3) and therefore can be expected to be a robust effect across a wide variety of cell types with varied heterochromatin levels.

The central coalescence of heterochromatin driven by flexibility can be energetically easily overcome: heterochromatin localizes near the NE, as is seen in most cell types, for weak NE-heterochromatin attractions comparable to thermal energy k_BT. This, plus the feature that the segregation profiles are spread across the whole nucleus, indicate that our flexibility-driven segregation effect is more akin to a NE-surface-driven adsorption effect than a bulk phase transition. For the latter, we expect to see sharp interfaces [63] between the inner and outer regions rather than the gradual segregation observed in our simulations. When there is a small free energy difference between the localization of monomers near or away from the inner NE, we observe segregation, which can demonstrate how easily it can be overwhelmed by the relatively weak attraction of heterochromatin to the NE [Fig. 2(c)].

A fundamental question is whether heterochromatin is less flexible than euchromatin. The average persistence length values of naked double-stranded DNA and loose chromatin lie in the broad range of values $l_P^{\mathrm{euc}} \approx 30$–$100$ nm. In contrast, this range is higher for condensed chromatin and $l_p^{\mathrm{htc}} \approx 100$–$400$ nm (Ref. [64] and references therein). These values suggest stiffness ratios ranging between $K/\epsilon \approx 1$–10. There is also a growing skepticism concerning the existence of a relatively stiffer 30-nm heterochromatin fiber *in vivo* [65]. In parallel, research into the liquid-like structure of heterochromatin-rich domains [66] reports surprising similarities with melts of flexible polymers. Hence, one may think that both chromatin types are simply mechanically indistinguishable. However, nuclear biochemical processes (e.g., histone modifications and DNA methylation) can affect the relative physical proximity between adjacent nucleosomes along the chromatin polymer by forming tightly packed heterochromatin or loosely packed euchromatin sections [4,5,30,67,68]. Within the heterochromatin, positional fluctuations of nucleosomes can be suppressed by neighboring nucleosomes [3,31]. The extent of this suppression, particularly in the transverse direction of the chromatin main axis, is weaker for euchromatin as compared to heterochromatin, potentially making euchromatin effectively more flexible than heterochromatin [2], and thus, can underlie the mechanism we demonstrate here.

The segregation mechanism demonstrated here could be used by cells to dynamically organize their nuclear architecture. Specifically, cells could use the suppressed flexibility of heterochromatin to save energy in processes that require rearrangement of nuclear content. For instance, in the absence of NE-chromatin attractions, heterochromatin readily segregates to the interior and promotes the formation of a single heterochromatin-rich domain [6,28]. Note that increasing chromatin stiffness and surface attraction (of heterochromatin) both lead to a similar degree of localization towards the periphery at similar chromatin densities and heterochromatin contents (Figs. 4 and 5). As f decreases (i.e., less heterochromatin), surface attraction becomes more efficient in terms of localizing chains to the periphery, possibly due to undersaturation of the surface by chromatin segments.

We note that an analogous mechanism may be at play as the cell enters mitosis, and chromatin is lengthwise compacted into thicker "fibers" [69,70]. It is reasonable to hypothesize that, with the breakage of chromatin-NE contacts followed by increasing the lengthwise compaction of chromosomes, which boosts their bending stiffnesses, the centers of masses of the chromosomes segregate towards the nuclear interior by the mechanism described here, where sister chromatids are located prior to cell division.

There are several caveats in our simulations that should be considered. One is that the relaxation time of the ring polymers could exceed the simulation period that we can achieve here due to topological polymer entanglements. Biologically, this high-entanglement scenario corresponds to relatively lower activity of topoisomerase II *in vivo* [71], which can result in chromosome relaxation times even longer than the duration of interphase [41]. However, the central heterochromatin coalescence that we demonstrate here could disappear in an ideal system where all chains are relaxed. In simulations where nonconcatenated rings are replaced by concatenated versions by allowing bond crossings, thus eliminating entanglements [72], we observe that the amount of heterochromatin in the nuclear interior further increases (Supplemental Material [46], Fig. S7). Since chains can mix quicker in the absence of entanglements [40], we conclude that the central heterochromatin coalescence shown here is not a side effect of unrelaxed chain conformations and will be more pronounced if topoisomerases are more active. Note that in our simulation, semiflexible heterochromatin prefers the interior but is also depleted from the periphery compared to flexible euchromatin (see Figs. 2–4). The volumetric regions near the periphery are larger than those in the interior. Thus, the total entropy change in the spherical confinement should favor an inverted chromatin organization, as observed in experimental studies [6,11,62].

Second, our NE interaction model assumes that heterochromatin can interact with the whole surface. In reality, there is a set of lamin-associated proteins providing such attachment [15]. Therefore, our model likely overestimates NE-chromatin contacts and underestimates the interaction strengths needed to keep the majority of the heterochromatin near the periphery. Nevertheless, the average size of the lamin-associated domain (LADs) is as large as a few million base pairs [23]. Thus, the anchoring effect of proteins on the inner surface of the NE, and resulting LADs, could be reasonably approximated by the whole-surface-attraction scheme used here. Further, in our simulations, for surface attraction strengths of ≈ 2–$3k_BT$ per bead, we obtain an average of ≈ 10 beads are in contact with the surface (Supplemental Material [46], Fig. S8), which is consistent with the $\approx N^{1/2}$ expected from the Gaussian estimate. This indicates that each heterochromatin segment is bound to the surface via ≈ 20–$30k_BT$, an intermolecular interaction sufficient to drive strong surface adsorption [73].

Lastly, our current study does not completely scan the whole parameter space for this problem. For instance, future studies might well vary the confinement radius R relative to both block sizes or persistence length. In addition, the

interplay between entropy and bending energy for different polymer architectures and stiffnesses is a large parameter space that would also be interesting for further studies. We also note that our conclusion that lamin-chromatin attraction is needed for the exterior arrangement of heterochromatin is, of course, subject to these additional parameters, as well as many others associated with the biological complexity of the problem at hand. Nevertheless, our study does show what can be expected from mainly entropically driven self-organization of confined polymers with varied stiffness.

B. Conditions for heterochromatin depletion from nuclear interior

Across varied chromatin concentrations and heterochromatin fractions, we systematically observe a higher concentration of heterochromatin than euchromatin in the nuclear interior, for heterochromatin that is slightly stiffer than euchromatin, and in the absence of heterochromatin-NE attraction (Figs. 2 and 3). We report two mechanisms that can reverse the central localization of heterochromatin and increase its peripheral concentration: (i) a large bending rigidity of heterochromatin compared to euchromatin (Fig. 4) and (ii) attraction between heterochromatin and the NE (Fig. 5). In the latter case, our simulations, which consider only nonspecific attractions, demonstrated how strong this effect can be even in cases where the strength of the attraction per monomer is relatively weak. The experimentally observed negative correlation between LBR expression levels and central heterochromatin coalescence are in accord with our model [26–28].

The high-bending stiffness mechanism (i) requires, in the absence of NE-chromatin attraction, a very high bending rigidity (i.e., the persistence length must be on the order of the nuclear dimensions) such that individual semiflexible chains are forced into bending and even buckling [60] (Fig. 4). Given that the persistence length of heterochromatin, l_p^{htc}, has been estimated to be at most several hundred nanometers [32], significantly lower than nuclear size, whether other mechanisms, such as molecular bridge formation [66] can effectively lead to a sufficiently large effective stiffness that has not been carefully studied but appears unlikely to be relevant *in vivo*. Notably, with the relatively weak persistence lengths considered in our study (i.e., much smaller than the polymer contour length or comparable to the confinement curvature as a limiting case), the type of angular potential used in the simulations should not qualitatively affect our results but rather show quantitative changes. The main reason for investigating FENE versus harmonic would be that the latter exhibits bond crossing (i.e., concatenation of chains), which is beyond the scope of the current work.

C. Interplay between flexibility-driven segregation and liquid-liquid phase separation

Given the complexity of the *in vivo* nuclear environment, the effect that we demonstrate here is unlikely to be the only factor driving heterochromatin-rich domain formation in the nuclear interior *in vivo*. Another factor likely to play a role is liquid-liquid phase separation [16,18,74,75]. Chromatin with heterochromatin markers H3K9me^{2,3} is bound by the epigenetic "reader" HP1 [17,66], which is likely to effectively drive attraction between heterochromatin-marked nucleosomes via HP1 dimerization or other complexation mechanisms [20]. Such attractions between heterochromatin segments are likely to amplify the central heterochromatin domain in the absence of NE-chromatin attraction by introducing two-body attractions between heterochromatin nucleosomes and possibly driving phase separation of heterochromatin from euchromatin [6,29]. The tendency for heterochromatin to already be segregated to the nuclear interior in the absence of interactions with the NE is a one-body driving force that can accelerate the actions of two-body interactions, further stabilizing the central localization of heterochromatin under weak NE-chromatin binding [28]. In our simulation results, neither heterochromatin nor euchromatin bears any attraction towards each other or themselves. This allowed us to unveil the effect of the flexibility difference between the two chromatin types in nuclear organization. We repeat some of our simulations with an attractive potential between heterochromatin beads, albeit by using a harmonic bond potential allowing bond crossing. Our simulations show that these interactions significantly increase the central coalescence of heterochromatin (see Supplemental Material [46], Fig. S9), further amplifying the heterochromatin inversion without NE-chromatin attraction [6]. This result indicates that any effect promoting the specific interactions between heterochromatin can work coherently with the stiffness-driven heterochromatin organization.

In conclusion, a coarse-grained polymer model considering the heteropolymer nature of chromosome chains demonstrated that a weak mechanical flexibility difference along the chromatin fiber could contribute to the experimentally observed local heterochromatin segregation. Furthermore, this segregation is independent of chromatin content and relative heterochromatin concentrations and can be reversed by weak ($\approx k_B T$) NE-heterochromatin attractions. Further questions that require study include the roles of more realistic heterochromatin distributions along chromosomes, inclusion of effects of sequence-specific nuclear proteins, the roles of varied protein concentrations in cellular confinement [76,77], and effects of the deformability of the NE [29,78] on chromatin organization. Given that random copolymer segregation can occur at the local level [10], chromosome structures, which are inherently random copolymers, can lead to the formation of local domains with different compositions resembling heterogeneities observed *in vivo*.

Data for the main text (simulation scipts, trajectory analysis, plotting) is available online at [79].

ACKNOWLEDGMENTS

This work was supported by the Alexander von Humboldt-Stiftung (AvH), and the Scientific and Technological Research Council of Turkey (TUBITAK) via Grant No. 122F309. We acknowledge computing resources from the Max-Planck Computational and Data Facilities (MPCDF). Work at NU was supported by NIH Grant No. R01-GM105847, subcontract to the University of Massachusetts under NIH Grant No. UM1-HG011536, and by the U.S. Department of Energy (DOE), Office of Basic Energy Sciences under Contract No. DE-FG02-08ER46539.

[1] R. D. Kornberg, Chromatin structure: A repeating unit of histones and DNA, Science **184**, 868 (1974).

[2] N. Kepper, D. Foethke, R. Stehr, G. Wedemann, and K. Rippe, Nucleosome geometry and internucleosomal interactions control the chromatin fiber conformation, Biophys. J. **95**, 3692 (2008).

[3] O. Müller, N. Kepper, R. Schöpflin, R. Ettig, K. Rippe, and G. Wedemann, Changing chromatin fiber conformation by nucleosome repositioning, Biophys. J. **107**, 2141 (2014).

[4] M. A. Ricci, C. Manzo, M. F. García-Parajo, M. Lakadamyali, and M. P. Cosma, Chromatin fibers are formed by heterogeneous groups of nucleosomes in vivo, Cell **160**, 1145 (2015).

[5] G. J. Thorn, C. T. Clarkson, A. Rademacher, H. Mamayusupova, G. Schotta, K. Rippe, and V. B. Teif, DNA sequence-dependent formation of heterochromatin nanodomains, Nat. Commun. **13**, 1861 (2022).

[6] M. Falk, Y. Feodorova, N. Naumova, M. Imakaev, B. R. Lajoie, H. Leonhardt, B. Joffe, J. Dekker, G. Fudenberg, I. Solovei, and L. A. Mirny, Heterochromatin drives compartmentalization of inverted and conventional nuclei, Nature (London) **570**, 395 (2019).

[7] M. D. Stefano, H.-W. Nützmann, M. A. Marti-Renom, and D. Jost, Polymer modelling unveils the roles of heterochromatin and nucleolar organizing regions in shaping 3D genome organization in Arabidopsis thaliana, Nucleic Acids Res. **49**, 1840 (2021).

[8] L. Leibler, Theory of microphase separation in block copolymers, Macromolecules **13**, 1602 (1980).

[9] M. O. de la Cruz, Theory of microphase separation in block copolymer solutions, J. Chem. Phys. **90**, 1995 (1989).

[10] B. W. Swift and M. O. de la Cruz, Random copolymers in concentrated solutions, Europhys. Lett. **35**, 487 (1996).

[11] G. Bajpai, D. Amiad Pavlov, D. Lorber, T. Volk, and S. Safran, Mesoscale phase separation of chromatin in the nucleus, eLife **10**, e63976 (2021).

[12] D. M. Gilbert, Nuclear position leaves its mark on replication timing, J. Cell Biol. **152**, F11 (2001).

[13] D. M. Carone and J. B. Lawrence, Heterochromatin instability in cancer: From the Barr body to satellites and the nuclear periphery, Semin. Cancer Biol. **23**, 99 (2013).

[14] A. Akhtar and S. M. Gasser, The nuclear envelope and transcriptional control, Nat. Rev. Genet. **8**, 507 (2007).

[15] Y. Y. Shevelyov and S. V. Ulianov, The nuclear lamina as an organizer of chromosome architecture, Cells **8**, 136 (2019).

[16] B. A. Gibson, L. K. Doolittle, M. W. G. Schneider, L. E. Jensen, N. Gamarra, L. Henry, D. W. Gerlich, S. Redding, and M. K. Rosen, Organization of chromatin by intrinsic and regulated phase separation, Cell **179**, 470 (2019).

[17] Q. MacPherson, B. Beltran, and A. J. Spakowitz, Bottom-up modeling of chromatin segregation due to epigenetic modifications. Proc. Natl. Acad. Sci. USA **115**, 12739 (2018).

[18] A. R. Strom, A. V. Emelyanov, M. Mir, D. V. Fyodorov, X. Darzacq, and G. H. Karpen, Phase separation drives heterochromatin domainformation, Nature (London) **547**, 241 (2017).

[19] F. Erdel, A. Rademacher, R. Vlijm, J. Tünnermann, L. Frank, R. Weinmann, E. Schweigert, K. Yserentant, J. Hummert, C. Bauer *et al.*, Mouse heterochromatin adopts digital compaction states without showing hallmarks of HP1-driven liquid-liquid phase separation, Mol. Cell **78**, 236 (2020).

[20] F. Erdel, Phase transitions in heterochromatin organization, Curr. Opin. Struct. Biol. **80**, 102597 (2023).

[21] F. Erdel and K. Rippe, Formation of chromatin subcompartments by phase separation, Biophys. J. **114**, 2262 (2018).

[22] B. van Steensel and A. S. Belmont, Lamina-associated domains: Links with chromosome architecture, heterochromatin, and gene repression, Cell **169**, 780 (2017).

[23] L. Guelen, L. Pagie, E. Brasset, W. Meuleman, M. B. Faza, W. Talhout, B. H. Eussen, A. de Klein, L. Wessels, W. de Laat, and B. van Steensel, Domain organization of human chromosomes revealed by mapping of nuclear lamina interactions, Nature (London) **453**, 948 (2008).

[24] J. C. Harr, T. R. Luperchio, X. Wong, E. Cohen, S. J. Wheelan, and K. L. Reddy, Directed targeting of chromatin to the nuclear lamina is mediated by chromatin state and A-type lamins, J. Cell Biol. **208**, 33 (2015).

[25] M. Zwerger, C. Y. Ho, and J. Lammerding, Nuclear mechanics in disease, Annu. Rev. Biomed. Eng. **13**, 397 (2011).

[26] A. L. Olins, G. Rhodes, D. B. M. Welch, M. Zwerger, and D. E. Olins, Lamin B receptor: Multi-tasking at the nuclear envelope. Nucleus **1**, 53 (2010).

[27] I. Solovei, M. Kreysing, C. LanctOt, S. KOsem, L. Peichl, T. Cremer, J. Guck, and B. Joffe, Nuclear architecture of rod photoreceptor cells adapts to vision in mammalian evolution, Cell **137**, 356 (2009).

[28] I. Solovei, A. S. Wang, K. Thanisch, C. S. Schmidt, S. Krebs, M. Zwerger, T. V. Cohen, D. Devys, R. Foisner, L. Peichl *et al.*, LBR and lamin A/C sequentially tether peripheral heterochromatin and inversely regulate differentiation, Cell **152**, 584 (2013).

[29] A. G. Attar, J. Paturej, E. J. Banigan, and A. Erbaş, Chromatin phase separation and nuclear shape fluctuations are correlated in a polymer model of the nucleus, Nucleus **15**, 2351957 (2024).

[30] S. Baldi, P. Korber, and P. B. Becker, Beads on a string—Nucleosome array arrangements and folding of the chromatin fiber, Nat. Struct. Mol. Biol. **27**, 109 (2020).

[31] S. S. Ashwin, T. Nozaki, K. Maeshima, and M. Sasai, Organization of fast and slow chromatin revealed by single-nucleosome dynamics, Proc. Natl. Acad. Sci. USA **116**, 19939 (2019).

[32] K. Rippe, Making contacts on a nucleic acid polymer, Trends Biochem. Sci. **26**, 733 (2001).

[33] J. Langowski, Polymer chain models of DNA and chromatin, Eur. Phys. J. E **19**, 241 (2006).

[34] H. D. Ou, S. Phan, T. J. Deerinck, A. Thor, M. H. Ellisman, and C. C. O'Shea, ChromEMT: Visualizing 3D chromatin structure and compaction in interphase and mitotic cells, Science **357**, eaag0025 (2017).

[35] C. Singh, M. Goulian, A. J. Liu, and G. H. Fredrickson, Phase behavior of semiflexible diblock copolymers, Macromolecules **27**, 2974 (1994).

[36] F. S. Bates and G. Fredrickson, Conformational asymmetry and polymer-polymer thermodynamics, Macromolecules **27**, 1065 (1994).

[37] S. Mao, Q. MacPherson, J. Qin, and A. J. Spakowitz, Field-theoretic simulations of random copolymers with structural rigidity, Soft Matter **13**, 2760 (2017).

[38] P. R. Cook and D. Marenduzzo, Entropic organization of interphase chromosomes, J. Cell Biol. **186**, 825 (2009).

[39] L. A. Mirny, The fractal globule as a model of chromatin architecture in the cell, Chromosome Res. **19**, 37 (2011).

[40] J. D. Halverson, J. Smrek, K. Kremer, and A. Y. Grosberg, From a melt of rings to chromosome territories: The role of topological constraints in genome folding, Rep. Prog. Phys. **77**, 022601 (2014).

[41] A. Rosa and R. Everaers, Structure and dynamics of interphase chromosomes, PLoS Comput. Biol. **4**, e1000153 (2008).

[42] K. Kremer and G. S. Grest, Dynamics of entangled linear polymer melts: A molecular-dynamics simulation, J. Chem. Phys. **92**, 5057 (1990).

[43] S. de Nooijer, J. Wellink, B. Mulder, and T. Bisseling, Non-specific interactions are sufficient to explain the position of heterochromatic chromocenters and nucleoli in interphase nuclei, Nucleic Acids Res. **37**, 3558 (2009).

[44] H. S. Ashbaugh and H. W. Hatch, Natively Unfolded protein stability as a coil-to-globule transition in charge/hydropathy space, J. Am. Chem. Soc. **130**, 9536 (2008).

[45] M. J. Stevens, Simple simulations of DNA condensation, Biophys. J. **80**, 130 (2001).

[46] See Supplemental Material at http://link.aps.org/supplemental/10.1103/PhysRevE.110.014403 for benchmarking results, persistence-length calculations, additional analyses, and a short discussion on the nematic phases.

[47] J. A. Anderson, C. D. Lorenz, and A. Travesset, General purpose molecular dynamics simulations fully implemented on graphics processing units, J. Comput. Phys. **227**, 5342 (2008).

[48] J. Glaser, T. D. Nguyen, J. A. Anderson, P. Lui, F. Spiga, J. A. Millan, D. C. Morse, and S. C. Glotzer, Strong scaling of general-purpose molecular dynamics simulations on GPUs, Comput. Phys. Commun. **192**, 97 (2015).

[49] M. Girard, A. Ehlen, A. Shakya, T. Bereau, and M. O. de la Cruz, Hoobas: A highly object-oriented builder for molecular dynamics, Comput. Mater. Sci. **167**, 25 (2019).

[50] A. Stukowski, Visualization and analysis of atomistic simulation data with OVITO—The Open Visualization Tool, Model. Simul. Mater. Sci. Eng. **18**, 015012 (2010).

[51] W. Humphrey, A. Dalke, and K. Schulten, VMD: Visual molecular dynamics, J. Mol. Graphics **14**, 33 (1996).

[52] J. D. Halverson, W. B. Lee, G. S. Grest, A. Y. Grosberg, and K. Kremer, Molecular dynamics simulation study of nonconcatenated ring polymers in a melt. II. Dynamics, J. Chem. Phys. **134**, 204905 (2011).

[53] H. Dehghani, G. Dellaire, and D. P. Bazett-Jones, Organization of chromatin in the interphase mammalian cell. Micron **36**, 95 (2005).

[54] M. R. Branco and A. Pombo, Chromosome organization: New facts, new models, Trends Cell Biol. **17**, 127 (2007).

[55] S. Efroni, R. Duttagupta, J. Cheng, H. Dehghani, D. J. Hoeppner, C. Dash, D. P. Bazett-Jones, S. Le Grice, R. D. G. McKay, K. H. Buetow, T. R. Gingeras, T. Misteli, and E. Meshorer, Global transcription in pluripotent embryonic stem cells. Cell Stem Cell **2**, 437 (2008).

[56] R. Yu, B. McCauley, and W. Dang, Loss of chromatin structural integrity is a source of stress during aging, Hum. Genet. **139**, 371 (2020).

[57] I. D. Vladescu, M. J. McCauley, M. E. Nuñez, I. Rouzina, and M. C. Williams, Quantifying force-dependent and zero-force DNA intercalation by single-molecule stretching, Nature Methods **4**, 517 (2007).

[58] A. D. Stephens, E. J. Banigan, S. A. Adam, R. D. Goldman, and J. F. Marko, Chromatin and lamin A determine two different mechanical response regimes of the cell nucleus. Mol. Biol. Cell **28**, 1984 (2017).

[59] S. Kilic, A. L. Bachmann, L. C. Bryan, and B. Fierz, Multivalency governs HP1, Nat. Commun. **6**, 7313 (2015).

[60] A. Nikoubashman, D. A. Vega, K. Binder, and A. Milchev, Semiflexible polymers in spherical confinement: Bipolar orientational order versus tennis ball states, Phys. Rev. Lett. **118**, 217803 (2017).

[61] A. Maji, J. A. Ahmed, S. Roy, B. Chakrabarti, and M. K. Mitra, A Lamin-associated chromatin model for chromosome organization, Biophys. J. **118**, 3041 (2020).

[62] S. Shin, G. Shi, and D. Thirumalai, From effective interactions extracted using Hi-C data to chromosome structures in conventional and inverted nuclei, PRX Life **1**, 013010 (2023).

[63] C. Huang, M. O. de la Cruz, and B. W. Swift, Phase separation of ternary mixtures: Symmetric polymer blends, Macromolecules **28**, 7996 (1995).

[64] A. Brunet, N. Destainville, and P. Collas, Physical constraints in polymer modeling of chromatin associations with the nuclear periphery at kilobase scale, Nucleus **12**, 6 (2022).

[65] E. Fussner, R. W. Ching, and D. P. Bazett-Jones, Living without 30 nm chromatin fibers, Trends Biochem. Sci. **36**, 1 (2011).

[66] K. Hiragami-Hamada, S. Soeroes, M. Nikolov, B. Wilkins, S. Kreuz, C. Chen, I. A. De La Rosa-Velázquez, H. M. Zenn, N. Kost, W. Pohl *et al.*, Dynamic and flexible H3K9me3 bridging via HP1β dimerization establishes a plastic state of condensed chromatin, Nat. Commun. **7**, 11310 (2016).

[67] A. Routh, S. Sandin, and D. Rhodes, Nucleosome repeat length and linker histone stoichiometry determine chromatin fiber structure, Proc. Natl. Acad. Sci. USA **105**, 8872 (2008).

[68] A. Buckle, C. A. Brackley, S. Boyle, D. Marenduzzo, and N. Gilbert, Polymer simulations of heteromorphic chromatin predict the 3D folding of complex genomic loci, Mol. Cell **72**, 786 (2018).

[69] J. F. Marko, Linking topology of tethered polymer rings with applications to chromosome segregation and estimation of the knotting length, Phys. Rev. E **79**, 051905 (2009).

[70] A. Goloborodko, M. V. Imakaev, J. F. Marko, and L. Mirny, Compaction and segregation of sister chromatids via active loop extrusion, eLife **5**, e14864 (2016).

[71] S. M. Vos, E. M. Tretter, B. H. Schmidt, and J. M. Berger, All tangled up: How cells direct, manage and exploit topoisomerase function, Nat. Rev. Mol. Cell. Biol. **12**, 827 (2011).

[72] J. Farago, H. Meyer, J. Baschnagel, and A. N. Semenov, Mode-coupling approach to polymer diffusion in an unentangled melt. II. The effect of viscoelastic hydrodynamic interactions, Phys. Rev. E **85**, 051807 (2012).

[73] J. N. Israelachvili, *Intermolecular and Surface Forces*, rev. 3rd ed. (Academic Press, Burlington, MA, 2011).

[74] C. P. Brangwynne, P. Tompa, and R. V. Pappu, Polymer physics of intracellular phase transitions, Nat. Phys. **11**, 899 (2015).

[75] A. R. Strom, R. J. Biggs, E. J. Banigan, X. Wang, K. Chiu, C. Herman, J. Collado, F. Yue, J. C. R. Politz, L. J. Tait *et al.*, HP1α is a chromatin crosslinker that controls nuclear and mitotic chromosome mechanics, eLife **10**, e63972 (2021).

[76] A. Erbaş, M. O. de la Cruz, and J. F. Marko, Receptor-ligand rebinding kinetics in confinement, Biophys. J. **116**, 1609 (2019).

[77] Z. Koşar, A. G. Attar, and A. Erbaş, Facilitated dissociation of nucleoid-associated proteins from DNA in the bacterial confinement, Biophys. J. **121**, 1119 (2022).

[78] S. Seirin-Lee, F. Osakada, J. Takeda, S. Tashiro, R. Kobayashi, T. Yamamoto, and H. Ochiai, Role of dynamic nuclear deformation on genomic architecture reorganization, PLoS Comput. Biol. **15**, e1007289 (2019).

[79] https://doi.org/10.17617/3.P08YSZ.